The International Journal of Advanced Manufacturing Technology (2019) 102:3739–3746
https://doi.org/10.1007/s00170-019-03476-w

ORIGINAL ARTICLE

Improving hook characterization of friction stir lap welded Al alloy joint using a two-section stepped friction pin

R. Z. Xu[1] · S. L. Cui[1] · H. Li[1] · Y. X. Hou[1] · Z. C. Wei[1]

Received: 17 September 2018 / Accepted: 18 February 2019 / Published online: 26 February 2019

Abstract
Four millimeter-thick 7N01P Al alloy sheets were welded by friction stir lap welding (FSLW) with different tools at various welding heat inputs. Results showed that the highest load could be performed by the optimization of welding parameters using a traditional tool; but, the welding parameters had an obvious effect on the joint loads and fracture modes. The tools with the stepped sections, which could control stable material flow behavior at various welding parameters during FSLW, were introduced. The platform geometry of the stepped friction pin contained two types: one had a convex platform between two sections, and the other had a concave platform between two sections. The joints obtained by the tools with the stepped sections could have a stable load at different welding parameters. Especially, in comparison with the tool with a convex platform, the concave platform acted like a concave shoulder for second stepped pin, improving the material flow during the FSLW and realizing a sound joint with a relatively flat interface morphology, which insured the stability of the joint properties (from 5.2 kN to 5.9 kN) and fracture mode (shear mode) at various welding parameters.

Keywords Friction stir lap welding · 7N01P-T4 Al alloy · Material flow · Two-section stepped tool

1 Introduction

Friction stir welding (FSW) is a mature solid state joining method, which offers several advantages, such as small thermal deformation, no cracks, and energy conservation, and therefore has attracted special attention in welding of light metals [1, 2]. Many researchers have proved that the sound butt joints with high properties could be realized by FSW [3–5]. In recent years, it has been widely applied in aerospace, automotive, electronics, and ship-building industries [6, 7].

Lap joint is another important joint configuration besides the butt joint [8, 9]. However, the friction stir lap welding (FSLW) does not produce good quality welds with the same ease of the friction stir butt welding due to the formation of interface distortion, which has a significant effect on the strength of the lap joint, including the hook defect (HD) on the advancing side (AS) and the cold lap defect (CLD) on the retreating side (RS) [10–15].

✉ R. Z. Xu
rzxu@imr.ac.cn

[1] College of Material Science and Engineering, Shenyang Aerospace University, 37 Daoyi South Street, Shenyang 110136, China

Comparing with the CLD, the shape of HD is usually sharply upwards, reducing the effective sheet thickness [16], and at the same time, it can provide a beneficial orientation for crack propagation and cause the stress concentration [17]. Therefore, the HD is considered to be the most critical factor to the damage of joint performances, and the flat HD is generally considered to be the most favorable geometry for joint performances [18].

A lot of studies have proven that the parameters, such as welding speed and rotational rate, could change the HD shape [9, 10]. Since the relationship between the welding parameters and HD shape is quite complex and has not been fully understood, the HD shape is therefore very difficult to be controlled by the optimizing of welding parameters, which limits its industrial application [9–13, 19].

In addition, the different tool geometries can significantly influence the material flow and heat input during FSLW, resulting in the formation of various hook curves [6, 19]. Therefore, it is considered that designing the reasonable rotating tool pin to control the material flow is the most effective and simple method to improve the joint performance [20]. Many different tools had been selected for FSLW, but the tools did not control the behavior of material flow effectively. In this context, designing and preparing the welding tools,

Table 1 Chemical compositions of the A7N01 alloy (wt.%)

Material	Si	Fe	Cu	Mn	Mg	Zn	Ti	Al
A7N01	≤0.3	≤0.35	≤0.2	0.2–0.7	0.1–2.0	4.0–5.0	≤0.2	Bal.

aiming for achieving a stable interfacial morphology under a wide range of process parameters, is the focus of studying for the FSLW [21–23].

In this study, 7N01P-T4 Al alloy sheets with high properties were chosen as the base material for FSLW. The welding tools with different platform geometries were designed and prepared, in order to improve the HD shape of the FSLW joint. In addition, the welding was conducted under different welding heat inputs, aimed at evaluating the effect of the pin geometries on the stability of the interfacial morphology.

2 Experimental procedure

In this study, 4 mm-thick A7N01-T4 aluminum alloy sheets were selected as the base material, whose chemical compositions were listed in Table 1. All the welding operations consisted of two 300 mm × 150 mm sheets with an overlap width of 30 mm, and the welding were longitudinally introduced along the centerline of the overlap area, as shown in Fig. 1a and b. According to ISO 25239, the geometrical configurations for the FSLW specimen can be divided into two placements depending on whether the advancing side (AS) or the retreating side (RS) of the weld is near the top sheet edge. In this study, the configuration with the AS near the top sheet edge (Fig. 1c) was applied for FSLW, in order to evaluate the effect of HD geometry on the joint properties.

Three different FSW tools were designed and manufactured as shown in Fig. 2a. A schematic of their geometries and dimensions is shown in Fig. 2b–d. These three tools are defined as tools A, B, and C, respectively. Tool A is a traditional friction stir welding tool with a conical thread pin (Fig. 2b). Tools B and C are the new tools with two cylindrical stepped sections, and their platform shapes were convex and concave at the junction of the first and the second section (Fig. 2c and d), respectively. The FSLW operations were conducted with a constant traverse speed of 200 mm/min and at different tool rotating rates (800, 1400, and 2000 rpm) using different tools.

Specimens for metallographic examination were sectioned along the cross section of the weld. After being mechanically ground and polished, the specimens were etched with Keller's reagent consisting of 2 mL HF, 3 mL HCl, 5 mL HNO_3, and 190 mL H_2O. The microstructure at the interface was examined by an optical microscope (OM).

Lap-shear tensile specimens were cut by electrical discharge machining, with a length of 120 mm, a width of 10 mm and an overlap width of 30 mm (Fig. 1a). Shims were used at each end of the specimens to balance the offset axes of the lap specimens and minimize bending effects as shown in Fig. 1c. After being tested, the fracture locations were examined by OM.

3 Results and discussion

3.1 FSLW of Al alloy

Figure 3a–e shows the typical cross-section photographs of the FSLW joints with a constant welding speed of 200 mm/min using a traditional tool (tool A) under different rotational rates of 800, 1400, and 2000 rpm, respectively. It can be seen that all the HDs extended upwards, even though they were obtained by different rotational rates. With the rotational rate increasing, the upward trend of the HD was growing obviously as shown in Fig. 3b–f. In short, the effect of the welding parameter, i.e., the rotational rate, on the morphology and height of the HD was obvious and complex for FSLW using a traditional tool.

Figure 4a–e shows the typical cross-section photographs of the FSLW joints obtained by tool B. The FSLW operations using tools A and B were conducted at the same rotational rates. It is found that all the joints displayed the flat interface morphology, comparing with those prepared by tool A (Fig. 4b–f). However, the welding defects were detected in the joints at the high rotational rates (Fig. 4d and f). At a constant welding speed, the different rotational rates resulted in various thermal inputs in fact. In other words, the excessive high heat input had a deleterious effect on the joint properties.

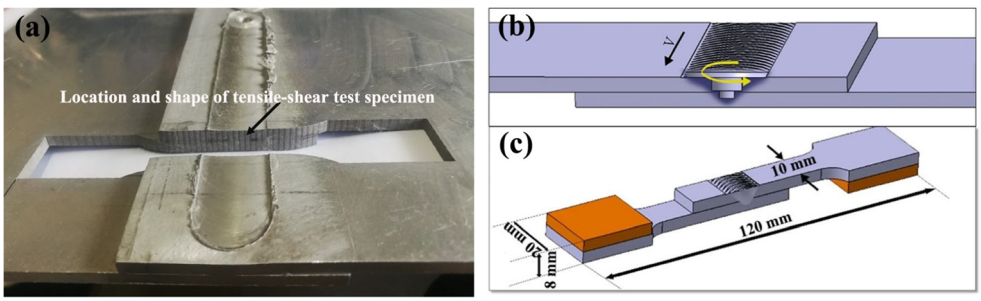

Fig. 1 (a) Lap configuration, (b) FSLW process, and (c) the of tensile-shear test specimen

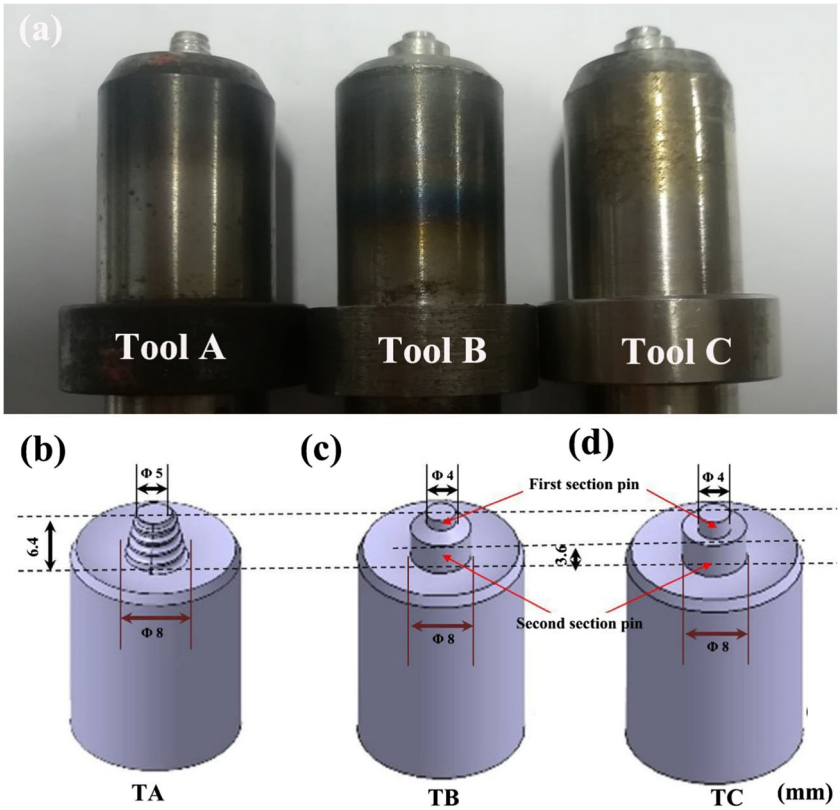

Fig. 2 (a) Three different tools and the schematics of their geometries and dimensions of different friction stir welding tools: (b) tool A, (c) tool B, and (d) tool C

Figure 5a–e shows the typical cross-section photographs of the FSLW joints using tool C. Similar to those of the joints obtained by tool B, the HDs were flat under the various welding parameters. Another important finding was that the joints obtained by tool C were sound even at a high rotating rate (Fig. 5d and f).

For FSLW Al alloy joints, the changing trend in the morphology of the HD would have a significant effect on their

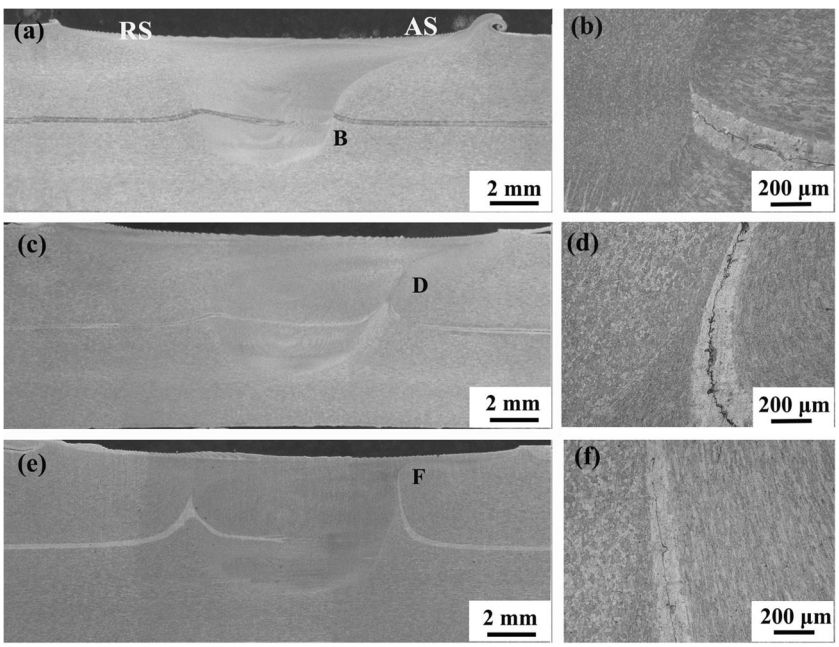

Fig. 3 (a), (c), and (e) cross-sectioned macrographs of FSLW joints and (b), (d), and (f) magnified micrographs of HDs using tool A at different rates: (a), (b) 800 rpm; (c), (d) 1400 rpm, and (e), (f) 2000 rpm

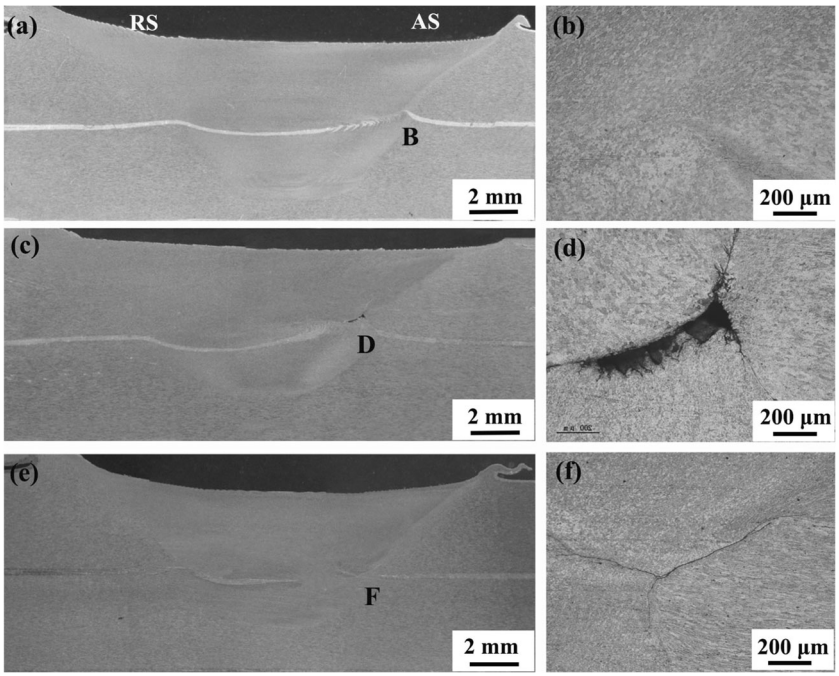

Fig. 4 (a), (c), and (e) cross-sectioned macrographs of FSLW joints and (b), (d), and (f) magnified micrographs of HDs using tool B at different rates: (a), (b) 800 rpm; (c), (d) 1400 rpm; and (e), (f) 2000 rpm

tensile-shear load and fracture mode, which will be discussed in the following sections.

3.2 Characteristics of fracture

The tensile-shear loads of FSLW A7N01-T4 joints obtained by three different tools under various rotational rates are shown in Fig. 6. The results indicated that the joints fabricated by the traditional tool (tool A) exhibited superior tensile-shear strength compared with the other two tools at 800 and 1400 rpm. However, with a further increasing rotational speed to 2000 rpm, the fracture load of the joint obtained by the traditional tool decreased significantly, indicating that the effect of welding parameters on the FSLW joint performance was obvious. It should be noted that the loads of the joint obtained by the other two tools were not the highest, but they were relatively more stable under different rotational rates, which would be beneficial for its practical application.

In order to further detect the effect of HD geometry on the tensile-shear load of the FSLW A7N01-T4 joint, the fracture

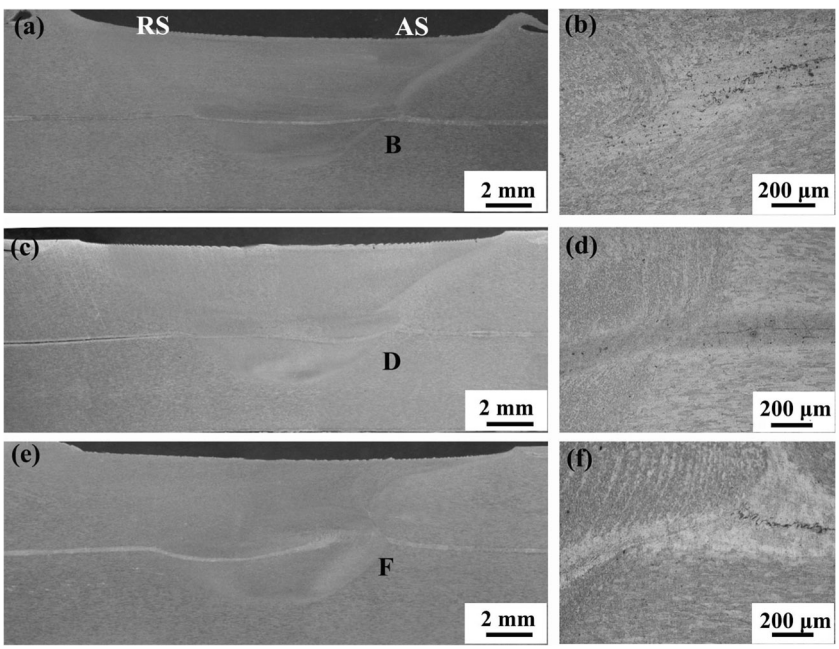

Fig. 5 (a), (c), and (e) cross-sectioned macrographs of FSLW joints and (b), (d), and (f) magnified micrographs of HDs using tool C at different rates: (a), (b) 800 rpm; (c), (d) 1400 rpm; and (e), (f) 2000 rpm

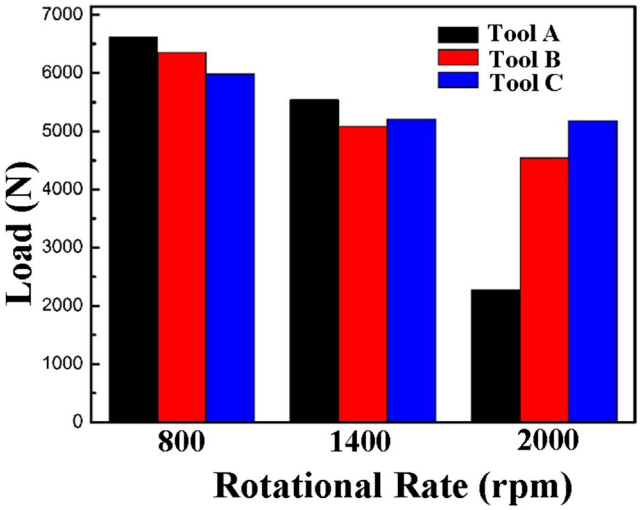

Fig. 6 Tensile-shear failure loads of FSLW joints prepared by three different tools under various rotational rates

locations were investigated (Figs. 7, 8, and 9). For the joints obtained by the traditional tool (tool A), the failure showed a shear fracture mode at the low rotational rates (800 and 1400 rpm) as shown in Fig. 7a–d. With a further increasing (2000 rpm), the fracture mode changed into a tensile fracture as shown in Fig. 7e and f. For the joints prepared by tools B and C, they exhibited the similar shear fracture mode (Figs. 8 and 9), in which the cracks firstly generated at the tip of HD, and then propagated along the lap interface (Figs.7a, 7b, 8, and 9), indicating the dominant effect of the effective bonding area on the joint properties. For the joints fractured in the tensile mode, the cracks also generated at the tip of HD, but then propagated upwards (Fig. 7e and f), which indicated that the effect of the effective sheet thickness on the lap joint performance was dominant.

The above results suggested that the interface morphology had a significant effect on the load and fracture mode of the FSLW joint. Hence, the stable interface morphology is essential to the stability of joint performance. In other words, the stepped tools (tools B and C) could successfully realize the control of stable interface morphology in the FSLW joint under various rotational rates, which would be important for the increasing application of FSLW.

3.3 Influencing mechanism of the pin geometries on the interfacial characteristics of joint

During FSLW, the different material flow behaviors resulted in the formation of different interface morphologies, and thus influenced the failure loads of the FSLW joint [13]. For the joints obtained by the traditional tool (tool A), the HDs bent upwards at the different welding parameters (Fig. 3) due to the action of the stir tool, which resulted in an obvious different joint load (Fig. 6). For the joint obtained by the tool B, there existed a material concentrated zone (MCZ) on the AS, and the material presented three different flow directions in this zone (Fig. 4). In addition, the flow behaviors were similar at the different welding parameters (Fig. 4b–f). For the joint obtained by the tool C, the material had a motion of downwards in the MCZ at the interface as shown in Fig. 5, indicating that the tool C could achieve a stable interfacial morphology at the various welding parameters.

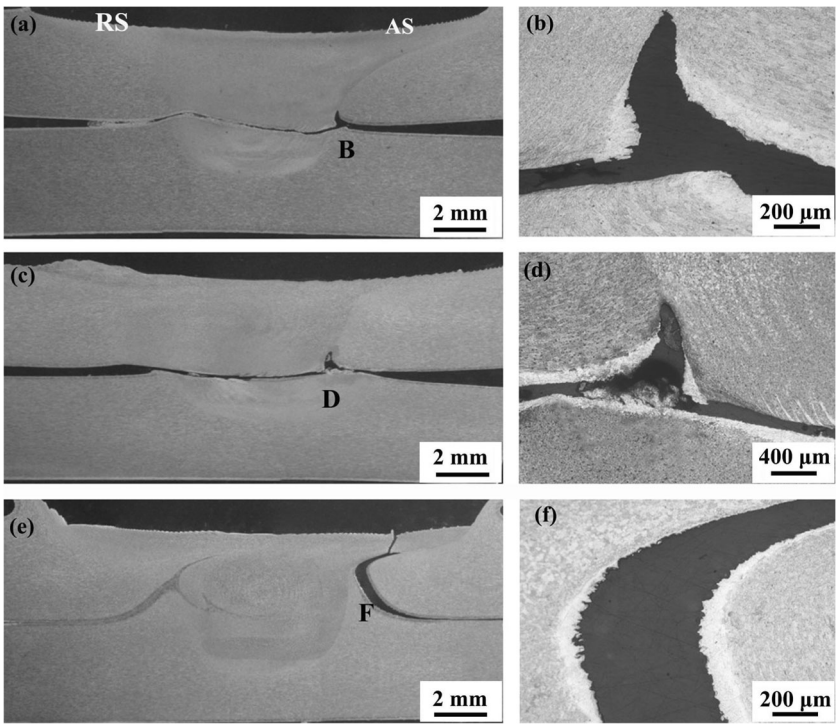

Fig. 7 (a), (c), and (e) typical fracture locations of FSLW joints and (b), (d), and (f) magnified micrographs using tool A at different rates: (a), (b) 800 rpm; (c), (d) 1400 rpm; and (e), (f) 2000 rpm

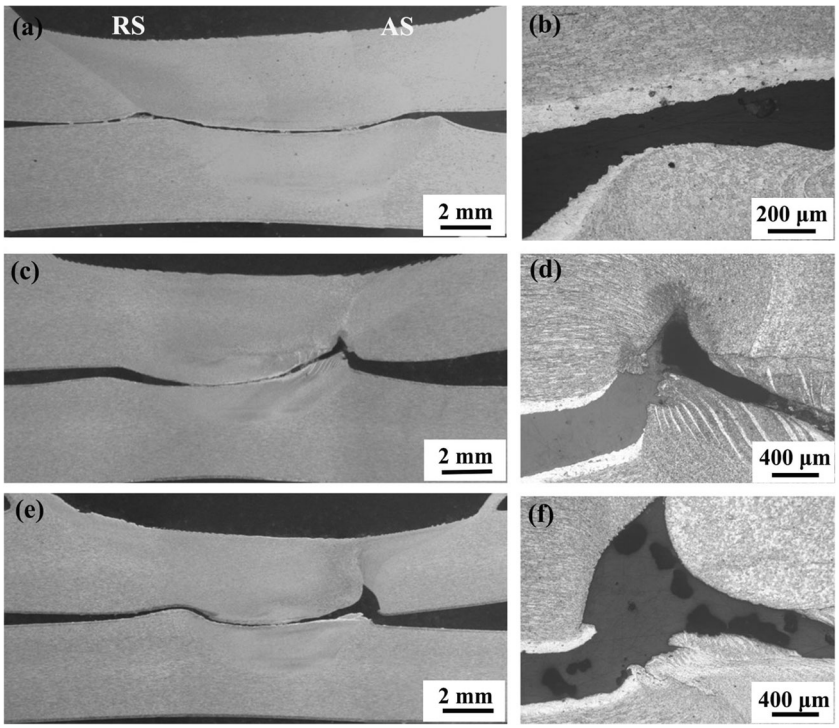

Fig. 8 (a), (c), and (e) typical fracture locations of FSLW joints and (b), (d), and (f) magnified micrographs using tool B at different rates: (a), (b) 800 rpm; (c), (d) 1400 rpm; and (e), (f) 2000 rpm

According to the above analysis, a schematic of material flow models of these three different tools during FSLW is provided in Fig. 10. For the FSLW joints using tool A, many studies have proven that the formation of the HD on the AS is mainly influenced by pin-driven material flow [12]. At first, the plasticized material was driven to the tip of the tool pin, leading to the formation of the MCZ. Subsequently, the MCZ pushed the adjacent material to transfer upwards, resulting in the upward-bending HD (Fig. 10a). However, for the CLD on the RS, it was the shoulder-driven material flow which could influence the CLD formation besides the pin-driven material flow [12]. Thus, the plasticized material driven by the shoulder flowed from the AS to the RS, and then moved downwards from the RS into the hole formed at the rear of tool,

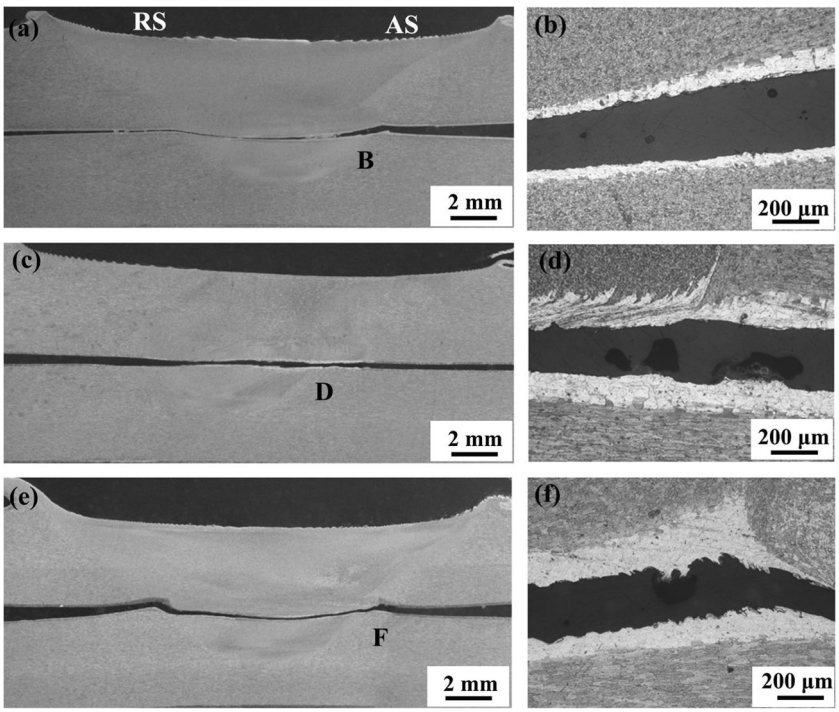

Fig. 9 (a), (c), and (e) typical fracture locations of FSLW joints and (b), (d), and (f) magnified micrographs using tool C at different rates: (a), (b) 800 rpm; (c), (d) 1400 rpm; and (e), (f) 2000 rpm

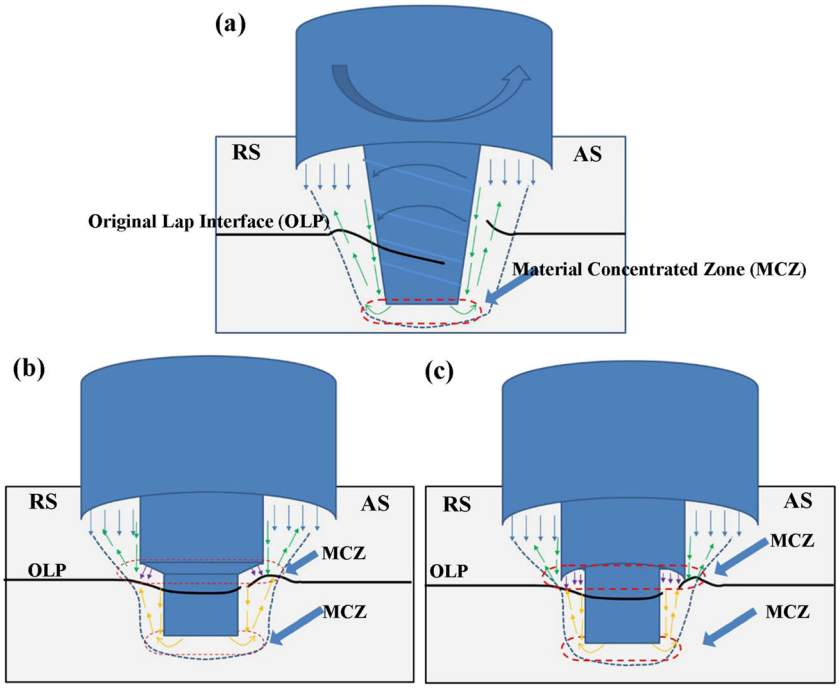

Fig. 10 Material flow schematics of different tools: (a) tool A, (b) tool B, and (c) tool C

subsequently pressed the CLD to migrate down [21]. Consequently, CLD on the RS extended into stir zone and displayed a morphology of firstly upward curve and then downward (Fig. 10a). With the increasing of the rotational speed, the material flow was more active, leading to the formation of a sharper interface morphology (Fig. 3e and f).

For the FSLW joints using tool B, the material flow was divided into two parts by the stepped pin, but the material flow trend was similar to that of using tool A (Fig. 10a and b). It should be noted that the first section of pin only plunged into the bottom of upper sheet and did not contact with the faying interface. The convex platform acted like a convex shoulder, which provided the pressure toward the lap interface, making another MCZ locate at the top of the lap interface. Besides, the MCZ formed by the rotating second section pin at the bottom of lower sheet pushing the adjacent material to transfer upwards, while the first section pin and its shoulder at the upper sheet pushed the material to transfer downwards (Fig. 10b). Based on the above analysis, it indicated that the material flow behavior was very complex at the lap interface, easily resulting in the welding defects, and specifically with an elevated rotational rate, the welding defects were detected (Fig. 4c–e).

For the FSLW joints using tool C, the material flow was also divided into two parts by the two-section stepped pin. However, differing from the tool B, the concave platform acted like a concave shoulder for the second stepped pin. It could serve as an escaping volume for the heated material and produce a compressive forging force for the lower sheet material, and the plastic deformation zone of the lower sheet was therefore more concentrated compared with that of the joint using the tool B (Fig. 10c). Consequently, the convection of plasticized material at the lap interface was much slighter than that of joint using tool B, reducing the welding defects effectively. Hence, the sound joints were obtained at various welding parameters (Fig. 5).

In short, the stable interface morphology was realized by controlling the material flow during FSLW using the two-section stepped pins at various heat inputs, which will be beneficial to obtain the weld joints with stable and reliable performances.

4 Conclusions

In this study, the feasibility of controlling the interlayer morphology by the two-section stepped pins during FSLW was verified, and the characteristics of their material flow were discussed. The following conclusions were drawn:

(1) For the traditional tool (tool A), changing the heat input has a significant effect on the modification of the interface morphology, resulting in the different fracture modes and joint performances. As the rotational speed increasing, the joint loads decreased and the fracture mode changed from shear fracture to tensile fracture, with the increasing upward trend of the HD.
(2) For the two-section stepped tool with a convex platform, the flat interface morphology was obtained during FSLW, but the complex material flow, which was induced by the action of pin and its convex platform,

leaded to the formation of welding defects at the lap interface easily.

(3) For the stepped tool with a concave platform between two sections, the concave platform acted like a concave shoulder for second stepped pin, improving the material flow and therefore forming a sound joint with a flat interface morphology, which insured the stability of joint properties (from 5.2 kN to 5.9 kN) and fracture mode (shear mode) at various heat inputs.

(4) The highest load could be obtained by the optimization of welding parameters using a traditional tool, but the welding parameters had an obvious effect on the joint loads and fracture modes. Comparing with traditional tool, the tool with the stepped sections could achieve a stable interfacial morphology under a wide range of process parameters, and therefore had a stable joint load, which was beneficial for the industrial application.

Funding information This study was supported by the National Natural Science Foundation of China under Grant No. 51601121, and Liaoning Province Science Foundation Program Nos. L201624 and 201602570.

References

1. Liu HJ, Zhao YQ, Hu YY, Chen SC, Lin Z (2015) Microstructural characteristics and mechanical properties of friction stir lap welding joint of alclad 7B04-T74 aluminum alloy. Int J Adv Manuf Technol 78:1415–1425
2. Zhao H, Shen Z, Booth M, Wen J, Fu L, Gerlich AP (2018) Calculation of welding tool pin width for friction stir welding of thin overlapping sheets. Int J Adv Manuf Technol 98:1721–1731
3. Ji SD, Meng XC, Li ZW, Ma L, Ga SS (2016) Investigation of vertical compensation friction stir-welded 7N01-T4 aluminum alloy. Int J Adv Manuf Technol 84:2391–2399
4. Rafiei R, Shamanian1 M, Fathi MH, Khodabakhshi F (2018) Dissimilar friction-stir lap-welding of aluminum-magnesium (AA5052) and aluminum-copper (AA2024) alloys: microstructural evolution and mechanical properties. Int J Adv Manuf Technol 94: 3713–3730
5. Mishra RS, Ma ZY (2005) Friction stir welding and processing. Mater Sci Eng R 50:1–78
6. Ge ZH, Gao SS, Ji SD, Yan DJ (2018) Effect of pin length and welding speed on lap joint quality of friction stir welded dissimilar aluminum alloys. Int J Adv Manuf Technol 98:1461–1469
7. Zhou ZL, Yue YM, Ji SD, Li ZW, Zhang LG (2017) Effect of rotating speed on joint morphology and lap shear properties of stationary shoulder friction stir lap welded 6061-T6 aluminum alloy. Int J Adv Manuf Technol 88:2135–2141
8. Xu RZ, Ni DR, Yang Q, Liu CZ, Ma ZY (2015) Influence of Zn interlayer addition on microstructure and mechanical properties of friction stir welded AZ31 mg alloy. J Mater Sci 50:4160–4173
9. Xu RZ, Ni DR, Yang Q, Liu CZ, Ma ZY (2016) Pinless friction stir spot welding of Mg–3Al–1Zn alloy with Zn interlayer. J Mater Sci Technol 32:76–88
10. Costa MI, Leitão C, Rodrigues DM (2017) Influence of post-welding heat-treatment on the monotonic and fatigue strength of 6082-T6 friction stir lap welds. J Mater Process Technol 250:289–296
11. Meng XC, Xu Z, Huang Y, Xie Y, Wang Y, Wan L, Lv ZL, Cao J (2018) Interface characteristic and tensile property of friction stir lap welding of dissimilar aircraft 2060-T8 and 2099-T83 Al-Li alloys. Int J Adv Manuf Technol 94:1253–1261
12. Liu HJ, Zhao YQ, Hu YY, Chen SX, Lin Z (2015) Microstructural characteristics and mechanical properties of friction stir lap welding joint of Al clad 7B04-T74 aluminum alloy. Int J Adv Manuf Technol 78:1415–1425
13. Song YB, Yang XQ, Cui L, Hou XP, Shen ZK, Xu Y (2014) Defect features and mechanical properties of friction stir lap welded dissimilar AA2024-AA7075 aluminum alloy sheets. Mater Des 55:9–18
14. Shirazi H, Kheirandish SH, Safarkhanian MA (2015) Effect of process parameters on the macrostructure and defect formation in friction stir lap welding of AA5456 aluminum alloy. Measurement 76: 62–69
15. Babu S, anaki Ram GD, Venkitakrishnan PV, Reddy M, Prasad Rao K (2012) Microstructure and mechanical properties of friction stir lap welded aluminum alloy AA2014. J Mater Sci Technol 28(5): 414–426
16. Jamshidi AH, Falahati NM (2017) Orbital friction stir lap welding in tubular parts of aluminium alloy AA5083. Sci Technol Weld Join 22:562–572
17. Liu HJ, Hu YY, Peng YX, Dou C, Wang ZG (2016) The effect of interface defect on mechanical properties and its formation mechanism in friction stir lap welded joints of aluminum alloys. J Mater Process Technol 238:244–254
18. Cao X, Jahazi M (2011) Effect of tool rotational speed and probe length on lap joint quality of a friction stir welded magnesium alloy. Mater Des 32:1–11
19. Vijay S, Eswar Y, Radovan K (2007) Investigation of the friction stir lap welding of aluminum alloys AA 5182 and AA 6022. J Mater Eng Perform 16:477–484
20. Emad S, Mohammad J, Alireza K, Hadi G (2016) Friction stir lap welding of 5456 aluminum alloy with different sheet thickness: process optimization and microstructure evolution. Int J Adv Manuf Technol 82:39–48
21. Liu Z, Zhou Z, Ji SD (2018) Improving interface morphology and shear failure load of friction stir lap welding by changing material concentrated zone location. Int J Adv Manuf Technol 95:4013–4022
22. Li Z, Yue Y, Ji SD, Chai, Zhou Z (2016) Joint features and mechanical properties of friction stir lap welded alclad 2024 aluminum alloy assisted by external stationary shoulder. Mater Des 90:238–247
23. Cantin GMD, David SA, Thomas WM, Lara-Curzio E, Babu SS (2005) Friction skew-stir welding of lap joints in 5083–0 aluminium. Sci Technol Weld Join 10:268–280